Electrochimica Acta 54 (2009) 7231–7235

Contents lists available at ScienceDirect

Electrochimica Acta

journal homepage: www.elsevier.com/locate/electacta

Electrochemical corrosion study of Sn–3Ag–3Cu solder alloy in NaCl solution

F. Rosalbino[a,*], E. Angelini[a], G. Zanicchi[b,c], R. Carlini[b,c], R. Marazza[b,c]

[a] Dipartimento di Scienza dei Materiali e Ingegneria Chimica, Politecnico di Torino, Corso Duca degli Abruzzi 24 - 10129 Torino, Italy
[b] Dipartimento di Chimica e Chimica Industriale, Università di Genova, Via Dodecaneso 31 - 16146 Genova, Italy
[c] Genoa Research Unit of the National Consortium of Materials Science and Technology (INSTM), Italy

ARTICLE INFO

Article history:
Received 26 March 2009
Received in revised form 4 June 2009
Accepted 11 July 2009
Available online 17 July 2009

Keywords:
Pb-free alloys
NaCl solution
Polarization curves
Electrochemical impedance spectroscopy (EIS)
Tin oxyhydroxychlorides

ABSTRACT

The corrosion behaviour of Sn–3Ag–3Cu (at%) alloy was investigated in 0.1 M NaCl solution by potentiodynamic polarization and impedance spectroscopy measurements and compared with that of the Sn–3Ag–0.5Cu (at%) solder employed in the packaging of some microelectronic components and devices. Scanning electron microscopy (SEM) and electron probe microanalysis (EPMA) were used to characterize the samples prior to and after the electrochemical tests. Results showed that in NaCl solution the corrosion resistance of the Sn–3Ag–3Cu alloy was better than that of the Sn–3Ag–0.5Cu solder. The presence of tin oxychlorides or oxyhydroxychlorides was detected at the surface of both alloys investigated after the electrochemical tests. The better corrosion behaviour of the Sn–3Ag–3Cu alloy compared to the Sn–3Ag–0.5Cu solder can be ascribed to a more adherent and compact corrosion products layer.

1. Introduction

Due to the inherent toxicity of Pb and Pb-containing compounds, the elimination of Pb-containing solders in microelectronic industry will be a worldwide significant target in the coming years. The trend of higher circuit board component densities results in the decrease of microelectronic packaging dimensions and the solder bump sizes; and the importance of soldering in microelectronics packaging is increasing because the microelectronics industry has made rapid development in recent years. Since the typical Pb-containing solders such as $Sn_{63}Pb_{37}$ have low cost, low melting temperature, very good wetting properties on substrates such as Cu, Ag, Pd, Au, and excellent mechanical properties, the Pb-containing solder alloys have been in use in microelectronics industry for a long time. The toxicity of Pb to the environment and consequent health hazards were an incentive to find suitable replacements of lead in the Pb-containing solder alloys without impairing the physical–chemical properties of the soldered joints [1–6]. In the present scenario, near-eutectic Sn–Ag–Cu (SAC) alloys have been considered very good candidates for substituting the Pb-containing solders in microelectronic packaging and interconnects [7–10]. The Sn–3Ag–0.5Cu solder alloy is beginning to come into use in the packaging of some microelectronic components and devices. As the metallurgical interconnecting and electrical continuity material of microelectronic products, lead-free solder alloys play a crucial part in governing the reliability of high performance packaging of microelectronic devices for long-term use. Compared with the Sn–Ag solder alloys, the Sn–3Ag–0.5Cu solder has a lower melting temperature, good wetting ability and better mechanical properties [11–13].

Very little information is available on the corrosion resistance of Sn–Ag–Cu solder alloys [14,15]. Polarization studies [14] performed by the present authors on Sn–3Ag–*x*Cu alloys in 0.1 M NaCl solution revealed that the addition of Cu from 0.8 to 6.7 at% resulted in a significant improvement of the corrosion resistance. The present work investigates the electrochemical corrosion behaviour of the Sn–3Ag–3Cu solder alloy by potentiodynamic polarization and impedance spectroscopy measurements performed in a chloride-containing environment. The electrochemical characterization of Sn–3Ag–0.5Cu alloy was also examined and a comparative study was made between the two alloys. Scanning electron microscopy (SEM) and electron probe microanalysis (EPMA) were used to obtain information about the surface composition of alloys after the electrochemical tests.

2. Experimental

Sn–3Ag–0.5Cu and Sn–3Ag–3Cu (at%) alloys were prepared by melting the stoichiometric amounts of pure elements (Sn and Ag, 99.999 mass% purity, both supplied by Newmet Koch, Waltham Abbey, England; Cu, 99.999 mass% purity, supplied by Ma Teck GmbH, Julich, Germany) in alumina crucibles, in an induction furnace under argon flow. The samples, enclosed under argon in

---

[*] Corresponding author. Tel.: +39 011 5644641; fax: +39 011 5644699.
E-mail address: francesco.rosalbino@polito.it (F. Rosalbino).

0013-4686/$ – see front matter © 2009 Elsevier Ltd. All rights reserved.
doi:10.1016/j.electacta.2009.07.030

Table 1
Microanalysis and crystallographic data of the alloys investigated.

Alloy nominal composition (at%)	Observed phases	Phase composition from EPMA (at%)	Crystal structure
Sn–3Ag–0.5Cu	(β Sn)	Sn 99.7.0 Cu 0.30	tI4-β Sn
	η (Cu_6Sn_5)	Cu 54.3 Sn 45.7	hP4-NiAs
	ε (Ag_3Sn)	Ag 73.8 Sn 25.4Cu 0.8	oP8-β Cu_3Ti
Sn–3Ag–3Cu	(β Sn)	Sn 99.8 Cu 0.20	tI4-β Sn
	η (Cu_6Sn_5)	Cu 54.4 Sn 45.6	hP4-NiAs
	ε (Ag_3Sn)	Ag 74.1Sn 25.2Cu 0.7	oP8-β Cu_3Ti

flame-sealed silica ampoules, were annealed for one week at 200 °C in a resistance furnace and then air-cooled. The microstructure of the alloys was investigated prior to and after the electrochemical measurements; light optical microscopy (LOM), scanning electron microscopy (SEM), and electron probe microanalysis (EPMA) based on energy dispersive X-ray spectroscopy, were used to check the overall composition of the different samples and analyse the coexisting phases. The microstructure of the alloys was investigated after preparing smooth surfaces of the specimen; the compositional contrast between the various phases was observed by means of a back-scattered electron (BSE) detector. For quantitative EPMA, the samples were analysed at 20 kV acceleration voltage using cobalt as standard for calibration of the beam current, gain and resolution of the spectrometer. Finally, the X-ray intensities were corrected for ZAF effects using pure elements as standards.

Electrochemical measurements were carried out in a single compartment cell using a standard three-electrode configuration: saturated calomel electrode (SCE) as a reference with a platinum electrode as counter and a sample as the working electrode. The surface area exposed to the test solution was 0.5 cm^2. The specimens were given a metallographic polishing prior to each experiment, followed by washing with distilled water and acetone. All the experiments were performed in aerated 0.1 M NaCl solution at room temperature (25 ± 0.1 °C). Potentiodynamic polarization curves were recorded in the potential range −1000 to +1000 mV vs. SCE reference electrode at a scan rate of 0.5 mV/s, after allowing a steady-state potential to develop. IR drop compensation was achieved using current interruption method. Measurements were carried out employing a Solartron 1286 Electrochemical Interface controlled by a personal computer. Electrochemical impedance was measured at the open circuit potential using a Solartron 1255 Frequency response Analyzer coupled to the Solartron 1286 Electrochemical Interface. The frequency range analysed went from 100 kHz up to 10 mHz, with the frequency values spaced logarithmically (seven per decade). The width of the sinusoidal voltage signal applied to the system was 10 mV rms (root-mean-square). Impedance measurements were performed at different exposure times in the aggressive environment.

Scanning electron microscopy and electron probe microanalysis were used to investigate the morphology and chemical composition of the alloys' surface after the electrochemical tests.

3. Results and discussion

3.1. Microstructural characterization

The nominal compositions of the lead-free solder alloys and the structural and compositional data obtained by EPMA of the phases observed are reported in Table 1.

Fig. 1 displays the microstructure of Sn–3Ag–0.5Cu alloy. The sample presents a typical three-phase appearance with a matrix of β Sn where Cu_6Sn_5 (black crystals) and Ag_3Sn (grey crystals with a needle shape) are dispersed. The observed solubility of Ag in the η phase and of Cu in the ε phase are very small, likewise for the Cu and Ag solubility in Sn, in agreement with [14,16].

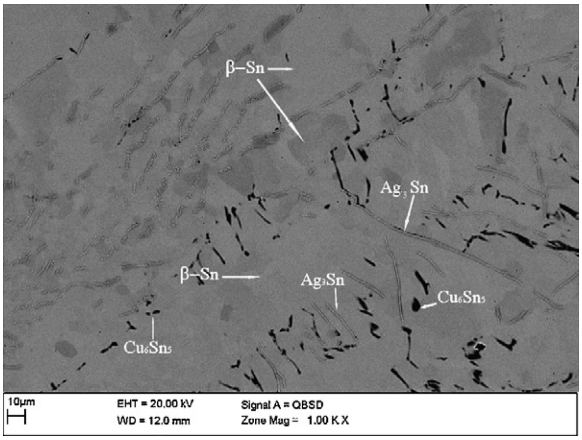

Fig. 1. SEM-BSE micrograph of the Sn–3Ag–0.5Cu solder alloy. Grey phase: (matrix): β Sn; black crystals: η phase (Cu_6Sn_5); grey elongated crystals: ε phase (Ag_3Sn). The compositions of the phases (at%) are obtained by EPMA.

The microstructure of Sn–3Ag–3Cu alloy is reported in Fig. 2. We can see in this sample the matrix of β Sn where many large crystals (black) of η phase Cu_6Sn_5 are precipitated and a few Ag_3Sn particles very finely dispersed in the matrix, similar to what was observed by [17].

3.2. Polarization curves

Potentiodynamic polarization curves and the relative rates of corrosion are reported in Fig. 3 recorded after 1 h immersion in 0.1 M NaCl solution, and data from these curves are summarised in Table 2.

Since all corrosion tests were performed in aerated NaCl solution, the cathodic branch of polarization curves may be ascribed to

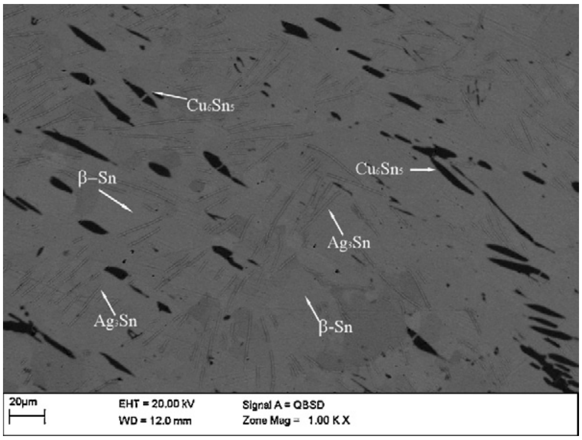

Fig. 2. SEM-BSE micrograph of the Sn–3Ag–3Cu solder alloy. Grey phase (matrix): β Sn with particles of Ag_3Sn finely dispersed; black crystals: η phase (Cu_6Sn_5). The compositions of the phases (at%) are obtained by EPMA.